Article



Adhesion strength between cells regulate nonmonotonic growth by a biomechanical feedback mechanism

Abdul N. Malmi-Kakkada, 1,* Sumit Sinha, 2 Xin Li, 3 and D. Thirumalai 3,*

¹Department of Chemistry and Physics, Augusta University, Augusta, Georgia; ²Department of Physics, University of Texas at Austin, Austin, Texas; and ³Department of Chemistry, University of Texas at Austin, Austin, Texas

ABSTRACT We determine how intercellular interactions and mechanical pressure experienced by single cells regulate cell proliferation using a minimal computational model for three-dimensional multicellular spheroid (MCS) growth. We discover that emergent spatial variations in the cell division rate, depending on the location of the cells either at the core or periphery within the MCS, is regulated by intercellular adhesion strength (f^{ad}). Varying f^{ad} results in nonmonotonic proliferation of cells in the MCS. A biomechanical feedback mechanism coupling the f^{ad} and microenvironment-dependent pressure fluctuations relative to a threshold value (p_c) determines the onset of a dormant phase, and explains the nonmonotonic proliferation response. Increasing f^{ad} from low values enhances cell proliferation because pressure on individual cells is smaller compared with p_c . However, at high f^{ad} , cells readily become dormant and cannot rearrange effectively in spacetime, leading to arrested cell proliferation. Utilizing our theoretical predictions, we explain experimental data on the impact of adhesion strength on cell proliferation and find good agreement. Our work, which shows that proliferation is regulated by pressure-adhesion feedback mechanism, may be a general feature of multicellular growth.

SIGNIFICANCE Adhesion between cells are primarily mediated by cadherin molecules, with E-cadherin expression in epithelial cells functioning as a tumor suppressor on the one hand but also as a promoter of tumor growth and metastasis. In physiological conditions, cells are characterized by heterogeneous intercellular adhesion strengths. This invites the question whether how adhesion favors or suppresses cell division depends on the strength of intercellular adhesion. Here, by using a computational model we show that cell-cell adhesion strength functions as a key mechanical regulator of cell division by integrating mechanical feedback on cell growth. On the basis of a simple assumption that cells detect forces from its microenvironment through intercellular adhesion forces we explain the surprising finding that varying adhesion strengths lead to nonmonotonic cell proliferation in 3D multicellular spheroids.

INTRODUCTION

Regulation of cell division is necessary for robust tissue growth and morphogenesis, with rapid cell proliferation being an integral phenotype characterizing early development and tumor growth (1,2). Mechanical forces influence cell division and cell spatial organization through mechano-sensitive processes (3–7). For instance, spatial constraints due to cell spatial packing limits cell proliferation (8–13). The spatiotemporal arrangement of cells in response to local

Submitted December 17, 2021, and accepted for publication April 26, 2022. *Correspondence: amalmikakkada@augusta.edu or dave.thirumalai@gmail.com

Editor: Baohua Ji.

https://doi.org/10.1016/j.bpj.2022.04.032

© 2022 Biophysical Society.

force (or stress) fluctuations arising from intercellular interactions, and how it controls cell proliferation, is unclear. Studies suggest (11,14–17) that the cross-talk between cell mechanical interactions and proliferation is mediated by cell-cell adhesion receptors.

An important mediator of intercellular adhesive force is a class of molecules called cadherins, which plays critical roles in morphogenesis, tissue healing, and tumor growth (18,19). The fundamental importance of cadherins in maintaining multicellular structure during morphogenesis is well known (20,21). Among the family of cell adhesion molecules, E-cadherin is the most abundant, and is expressed in most metazoan cohesive tissues (22,23). Mechanical coupling between the cortical cytoskeleton and cell membrane involves the cadherin cytoplasmic domain, with



forces exerted across the cell-cell contacts being transmitted between the cadherin extracellular domain and the cellular cytoskeletal machinery through the cadherin/catenin complex (24,25). Thus, to understand how adhesive forces control the spatial organization of cells within three-dimensional (3D) multicellular spheroid (MCS) and determine proliferation, we study the impact of varying intercellular adhesion strength on cell proliferation due to pressuredependent biomechanical feedback using a computational model.

We simulate an agent-based minimal model (see (26) for a review) for 3D MCS, where individual cells grow, move in response to intercellular forces, undergo division, and dynamically enter into a dormant phase as dictated by local pressure fluctuations. We show that variation in cell-cell adhesion strength, f^{ad} , results in nonmonotonic growth of the MCS into the surrounding medium. We discover that the pressure experienced by individual cells due to mechanical interactions with their neighbors quantitatively explains the nonmonotonic proliferation pattern. The f^{ad} parameter is a proxy for cell-cell adhesion strength, which could vary due to either changes in the cadherin expression level, cadherin clustering (27), increasing time of contact between cells (27), or "mechanical polarization," where cells reorganize their adhesive and cytoskeletal machinery to suppress actin density along cell-cell contact interfaces (28,29). By building on the integral feedback mechanism that couples cell dormancy and local pressure (6,7,11), we show that the pressure exerted by cells on one another explains the experimentally observed nonmonotonic cell collective growth as f^{ad} is varied from a low to a high value. The proposed mechanism could be a general attribute of MCS growth.

METHODS

We simulate the collective movement of cells using a minimal model of an evolving tumor embedded in a matrix using an agent-based 3D model (30-33). The cells, embedded in a highly viscous material mimicking the extracellular material, are represented as soft, spherical objects that interact via direct elastic (repulsive) and adhesive (attractive) forces.

Cell-to-cell and cell-to-matrix damping account for the effects of friction due to other cells, and the extracellular matrix, such as the collagen matrix. The model explicitly accounts for apoptosis, cell growth, and division. We also implicitly take into account the ability of individual cells to transition from growth to dormant phase depending on the local pressure. Thus, the collective motion of cells is determined by systematic cell-cell forces and the dynamics due to stochastic cell birth and apoptosis subject to a free boundary condition. The details of the models are presented in the supporting material plus our previous work (34-37).

Assessment of the values of f^{ad}

We estimated the f^{ad} from the typical strength of cell-cell attractive interactions reported in previous experimental studies to assess if they are in the reasonable range. Early experiments showed that the interaction strength between cell adhesion proteoglycans is $\sim 2 \times 10^{-5} \mu N / \mu m^2$ (38). Recently, single-cell force spectroscopy has been used to measure the typical forces required to rupture E-cadherin-mediated bonds between cells (39).

A typical force-distance curve (FDC), a plot of F_{ij} (the intercellular force) versus $|\mathbf{r}_i - \mathbf{r}_i|$ from Eq. S1 and the elastic force, is shown in Fig. 1 A. The plot shows that, for typical cell sizes (radius $\sim 5 \mu m$), the minimum force is $\approx 2 \times 10^{-4} \mu N$, which is fairly close to the experimental values of $\approx 1.5 \times 10^{-4} \mu N$ in Fig. 1 B and $4 \times 10^{-4} \mu N$ reported elsewhere (38). The inset in Fig. 1 B shows the work (the area under the FDC) required to overcome the intercellular adhesion force. The value of work done $\approx 0.78 \times 10^{-16}$ Nm for primordial germ cells (PGCs in *Xenopus laevis* embryo) is comparable with experiment, and accords well with the energy 1.25×10^{-16} Nm required to rupture the adhesive forces between two cells used in the simulations. Note that we did not adjust any parameters to obtain reasonable agreement.

Dependence of cell-cell contact length (l_c) and contact angle (β) on f^{ad}

Based on the center-to-center distance, $r_{ij} = |\mathbf{r}_i - \mathbf{r}_j|$, between cells i and j, and the contact length, l_c , the contact angle between two adhering cells, β , can be calculated (see inset Fig. 1 C for the definition). Let x be the distance from center of cell i to contact zone marked by l_c , along r_{ii} . Similarly, we define y as the distance between the center of cell j to l_c , once again along r_{ij} (Fig. 1 C). Based on the right triangle between x, R_i , and $l_c/2$, $R_i^2-x^2=R_j^2-y^2=(l_c/2)^2$ and $x+y=r_{ij}$, we obtain,

$$l_c = 2\sqrt{\frac{4r_{ij}^2R_i^2 - \left(r_{ij}^2 + R_i^2 - R_j^2\right)^2}{4r_{ij}^2}},$$
 (1)

$$\beta = \arctan(2y/l_c). \tag{2}$$

The probability distributions for l_c and β from the simulation as f^{ad} are varied, as shown in Fig. 1, C and D. The extent of the overlap between cells increase as f^{ad} increases, leading to enhanced jamming at higher adhesion strengths. The distribution of β (see Fig. 1 D), whose width increases at higher adhesion strength, shows that the mean angle value decreases with f^{ad} . By noting that $\beta + \frac{\theta_e}{2} = \frac{\pi}{2} (\theta_e)$ is as defined previously (40,41)) we infer from the results in Fig. 1 D that $\frac{\theta_e}{2}$ should increase as f^{ad} increases. Indeed, this is precisely what was found in phase transition in the zebrafish blastoderm (see Fig. 4 C of (41), showing decreased connectivity with decreased cell-cell adhesion). Hence, on the basis of the agreement in the force magnitude and the contact angles between our simulation and experimental data as shown in Fig. 1, we conclude that the range of cell-cell adhesion strengths we use in the simulations is reasonable.

The dependence of the total cell-cell interaction force, F_{ij} , as a function of cell center-to-center distance at three different f^{ad} , values is shown in Fig. 2 A. Not unexpectedly, the location of the minimum in F_{ij} decreases upon increase in f^{ad} (see inset in Fig. 2 A). A schematic sketch of the enhanced adhesion with increasing f^{ad} , due to greater E-cadherin expression, is shown in Fig. 2 B.

Physical and biological variables

The interaction parameters characterizing the systematic forces between cells are the two elastic constants (modulus, E_i , and Poisson ratio, v_i), and f^{ad} . In addition, cell birth (k_b) and apoptotic rates (k_a) are required to describe the evolution of the MCS. The values of k_a and k_b depend on the complicated biology governing cell fate, which are taken as parameters

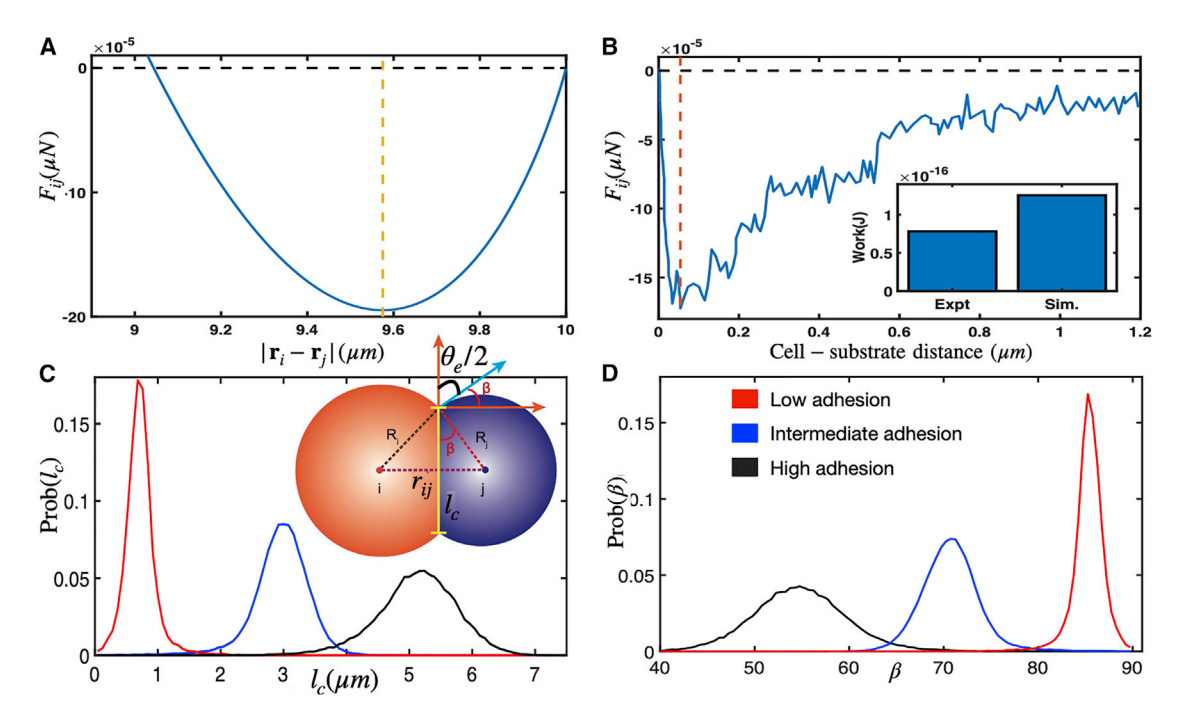


FIGURE 1 (A) Force on cell i due to j, F_{ij} , for $R_i = R_j = 5\mu m$ using mean values of elastic modulus, Poisson ratio, and receptor and ligand concentration (see Table S1). F_{ij} is plotted as a function of cell center-to-center distance $|\mathbf{r}_i - \mathbf{r}_j|$. We used $f^{ad} = 1.75 \times 10^{-4} \mu \text{N}/\mu \text{m}^2$ to generate F_{ij} . (B) Force-distance data extracted from single-cell force spectroscopy (SCFS) experiment (39). Inset shows the work required to separate cell and E-cadherin functionalized substrate in an SCFS experiment and in two cells in theory, respectively. Note that the unit Joules (J) is the same as Nm. Minimum force values are indicated by vertical dashed lines. (C) Probability distribution of contact lengths between cells for $f^{ad} = 0$ (red), $f^{ad} = 1.5 \times 10^{-4}$ (blue), and $f^{ad} = 3 \times 10^{-4}$ (black). Inset shows how cell-cell adhesion dictates the angle of contact between cells, β , and the length of contact, l_c . (D) Probability distribution of contact angles, β as a function f^{ad} . The color scheme is the same as in (C). To see this figure in color, go online.

in the simulations. In the simulations, we chose the $\frac{k_b}{k_c} \approx 20$ (see Table S1) to model rapid tumor growth.

If E_i , ν_i , and k_a are fixed, then tumor evolution is determined by f^{ad} and a specified threshold pressure, p_c . If the pressure on the i^{th} cell at a given time $(p_i(t))$ is less than p_c the cell grows and eventually divides. If $p_i(t) > p_c$, the cell enters the dormant phase (Fig. 2 C). We note parenthetically that $p_c \ge$ 0 is required for describing the time-dependent tumor growth law observed in experiments (see Fig. S1 A). The existence of p_c above which cell division is halted is in agreement with recent experiments (42). Here, we explore the effects of f^{ad} and p_i on tumor proliferation.

The minimal model considered here allows us to focus on elucidating how cell-cell adhesive interactions determine biomechanical feedback on cell proliferation. To explore a wide range of cell-cell adhesion strengths incorporating cell size growth we consider a minimal but realistic model.

RESULTS

Cell proliferation depends nonmonotonically on cell-cell adhesion strength f^{ad}

We first quantify how changing f^{ad} impacts cell division, and hence the overall tumor growth. The simulations were initiated with 100 cells at t = 0, and the evolution of the cells is determined by the equations of motion, and the rules governing birth and apoptosis (see supporting material for a brief description). We performed simulations at different values of f^{ad} until ~ 7.5 days (= $12\tau_{min}$, where τ_{min} = k_h^{-1} is the average cell division time). The number of cells (N) as a function of f^{ad} , at various times in the range of $5\tau_{min}$ to $12\tau_{min}$ (with colors for time t in units of τ_{min}), are shown in Fig. 2 D. The central result, summarized in Fig. 2 D, shows that tumor proliferation depends nonmonotonically on f^{ad} . The tumor growth is enhanced as f^{ad} increases from small values, attains a maximum at f^{ad} = f_c^{ad} , and decreases as f^{ad} exceeds f_c^{ad} .

On increasing f^{ad} from 0 to $1.75 \times 10^{-4} \mu N/\mu m^2$, the total number of cells, N, at $t = 12\tau_{min}$ (~ 7.5 days; green in Fig. 2 D) increases substantially. At higher intercellular adhesion strengths $(f^{ad} > 1.75 \times 10^{-4})$, the proliferation capacity (PrC; quantified in terms of the total number of cells on day 7.5) is suppressed (Fig. 2 D). While N = 12,000 cells on day 7.5 at $f^{ad} =$ $1.75 \times 10^{-4} \mu \text{N}/\mu \text{m}^2$, at higher f^{ad} values (such as $3 \times$ $10^{-4} \mu N/\mu m^2$), the tumor consists of only 4000 cells at the same time t. The surprising nonmonotonic dependence of N on f^{ad} is qualitatively consistent with recent experiments (39,43,44), as we discuss below.

Competition between local pressure and jamming drives nonmonotonic proliferation

The nonmonotonic tumor proliferation may be understood from the following physical arguments. Proliferation

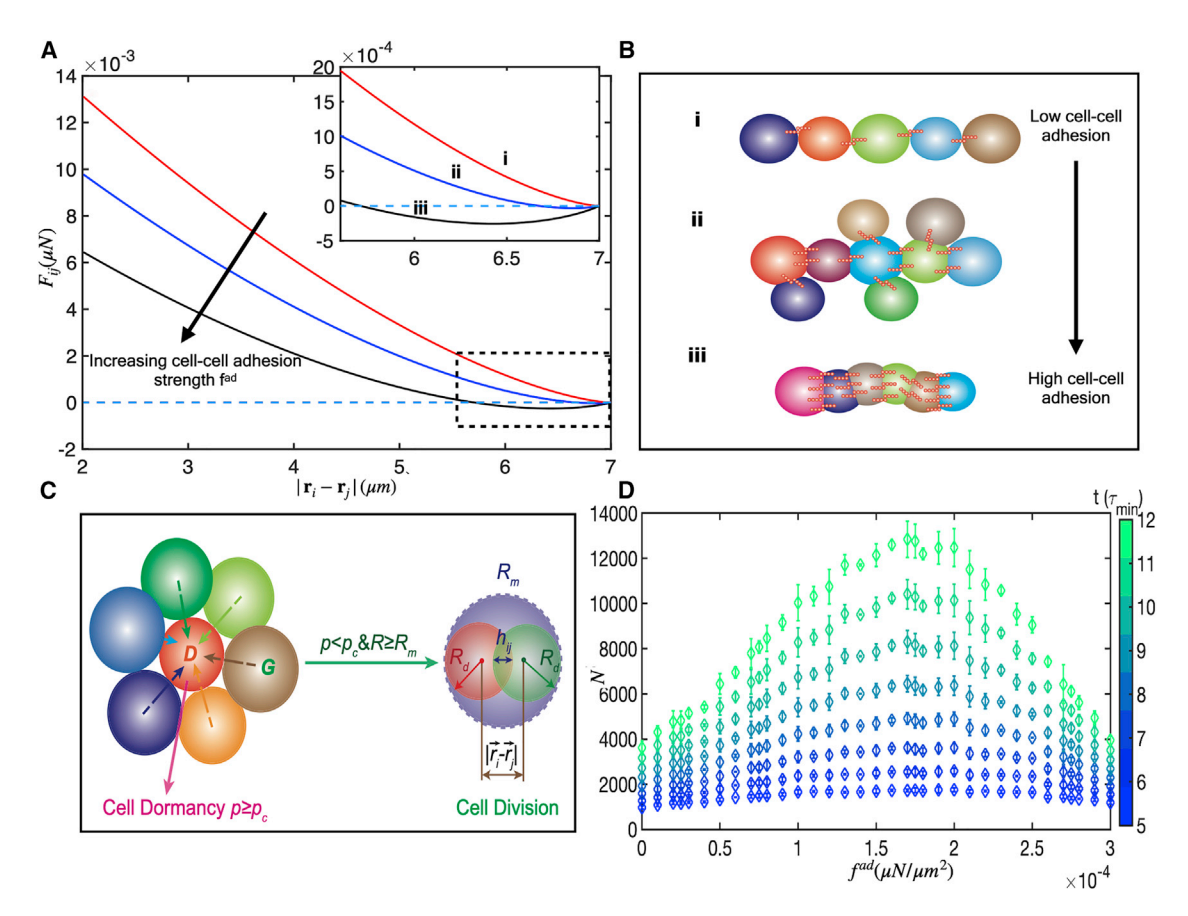


FIGURE 2 Forces and nonmonotonic growth of the MCS. (A) The interaction force, F_{ij} , between cells as a function of cell center-to-center distance. As f^{ad} increases, the magnitude of the adhesive force increases. Inset shows the regime highlighted in the dashed box where f^{ad} increases from i (weakest) to iii (strongest). (B) Impact of three different regimes of f^{ad} on the spatial arrangement of the cells. Cadherin molecules are represented as short red bonds. The three adhesive regimes in the simulations correspond to (i) low, (ii) intermediate, and (iii) high values of f^{ad} . (C) Cell dormancy (left) and cell division (right) in 3D cell collectives. If the local pressure p_i on the i^{th} cell (due to contacts with the neighboring cells) exceeds the critical pressure, p_C , the cell enters the dormant state, D. Otherwise, the cells undergo growth (G) until they reach the mitotic radius, R_m , when the cell divides into two identical cells with identical radii R_d . The value of R_d is determined to ensure that the total volume upon cell division is conserved. A cell that is dormant at a given time may transit from that state into growth phase at subsequent times. (D) Total number of cells (N), from $t = 5\tau_{min}$ to $12\tau_{min}$, at intervals of τ_{min} (= 54,000sec), as a function of f^{ad} for $p_c = 10^{-4}$ MPa. The nonmonotonic proliferation behavior is pronounced at $t=12 au_{min}$. Error bars here, and henceforth, are calculated from the standard deviation. The scale on the right gives time (t) in units of au_{min} . To see this figure in color, go online.

capacity is determined by the number of cells with pressure less than p_c . If the pressure on a cell exceeds p_c , it becomes dormant. Therefore, two factors should be considered in determining how mechanical feedback dictates cell proliferation: 1) dependence of intercellular pressure and 2) cell spatial packing, on f^{ad} . Because the average pressure on a cell depends on the magnitude of the net adhesive force, the cell pressure decreases at higher values of f^{ad} (see supporting material section I). This is similar to the pressure in real gases (van der Waals picture) in which the interparticle attraction leads to a decrease in the average pressure. Therefore, within a certain range of $f^{ad} \leq f_c^{ad}$, we expect the number of cells that is poised to divide should increase, causing enhanced tumor proliferation (van der Waals regime). At very high values of f^{ad} , however, the adhesive interactions becomes so strong that the number of nearest neighbors of a given cell increases (Fig. S2, A and B). This leads to an increase in pressure that decreases proliferation (jamming regime (6)). Because we are simulating a growing system where the number of cells increases with time, density is not an independent tuning parameter but is an emergent dynamical property that is linked to intercellular adhesion strength. From these arguments it follows that cell proliferation would increase with increasing f^{ad} at low cell-cell adhesion strengths. However, at high f^{ad} , cell proliferation would be limited due to a jamming effect.

The total average pressure (p_t) that a cell experiences is given by $p_t \sim \overline{n}_{NN} \langle p_1 \rangle$, where \overline{n}_{NN} is the mean number of nearest neighbor cells, and $\langle p_1 \rangle$ is the average pressure a neighboring cell exerts on a cell. We use simulations to estimate the dependence of \overline{n}_{NN} on f^{ad} (see Fig. S2, A and B). For cell i, the nearest neighbors are defined as cells with nonzero overlap ($h_{ii} > 0$; see Fig. 2 C for a visualization of

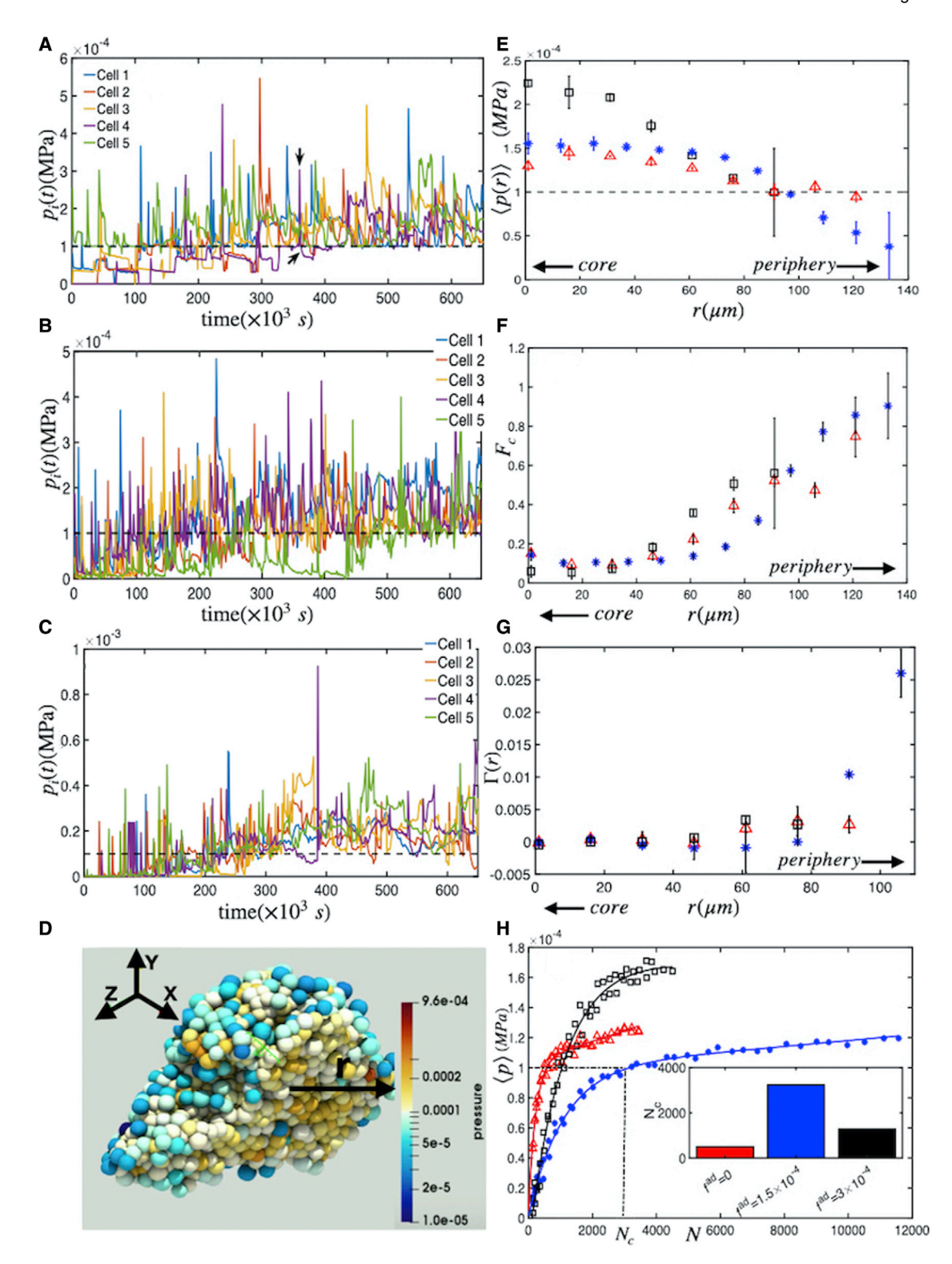


FIGURE 3 Temporal and spatial variations in pressure. Pressure as a function of time for selected individual cells at (A) $f^{ad}=0$, (B) $f^{ad}=1.5\times$ 10^{-4} , and (C) $f^{ad} = 3 \times 10^{-4}$. Dashed black lines correspond to the p_c value. Black arrows in (A) highlight p_i above p_c . (D) A cross section through a tumor spheroid with distance r from tumor center to periphery at $t \sim 12\tau_{min}$ for $f^{ad} = 0$. Typically, pressure decreases from the core to the periphery of the MCS. Color bar indicates pressure in units of MPa. (E) The average pressure experienced by cells at a distance r (µm) from the MCS center for $f^{ad}=0$ (red), $f^{ad}=1.5\times 10^{-4}$ (blue), and $f^{ad}=3\times 10^{-4}$ (black) (same symbols and color are used for F-H). The dashed line is $p_c=1.5\times 10^{-4}$ 10^{-4} MPa. Cells in the core are dormant with pressure above p_c . (F) The fraction of cells with $p < p_c$ as a function of r. At the tumor periphery cells

(legend continued on next page)

 h_{ij}). To obtain $\langle p_1 \rangle$, we expand around h_0 , the cell-cell overlap value, where both the attractive and repulsive interaction terms are equal $(h_{ij}|_{F_{ij}^{el}=F_{ij}^{ad}})$, corresponding to the overlap distance at which p=0 (see Fig. S1 B). By expanding to first order, the average pressure of a single cell is $\langle p_1 \rangle \approx \frac{\partial p_1}{\partial h}(h-h_0)$, where $h=\overline{h}_{ij}$ is the mean cell-cell overlap, dependent on f^{ad} (see Fig. S3). From the simulations, $h-h_0$ increases approximately linearly with f^{ad} (see Fig. S4), implying that high f^{ad} limits cellular position rearrangements.

To investigate how cell spatial arrangement affects intercellular pressure, we calculate the pressure gradient with respect to cell-cell overlap, $\frac{\partial p_1}{\partial h}$, using

$$p_1 = \frac{|F|}{A} \simeq \frac{Jh^{\frac{3}{2}} - Bf^{ad}h}{Ch},\tag{3}$$

$$\frac{\partial p_1}{\partial h} \simeq \frac{J}{2Ch_2^{\frac{1}{2}}}|_{h=h_0} = \frac{J}{2Ch_0^{\frac{1}{2}}},\tag{4}$$

to separate out the dependence of pressure on h_{ij} and f^{ad} . In Eqs. 3 and 4 J, B, and C are independent of cell-cell overlap (h) and f^{ad} . They are obtained from the definitions of elastic and adhesive forces and the definition of intercellular contact area, A_{ij} . The resulting expressions are: $J = 1 / \left[\frac{3}{4} \left(\frac{1 - v_i^2}{E_i} + \frac{1 - v_j^2}{E_j} \right) \sqrt{\frac{1}{R_i(t)} + \frac{1}{R_j(t)}} \right], \quad B = \left[\pi R_i R_j / (R_i + R_j) \right] \times \frac{1}{2} \left(c_i^{rec} c_j^{lig} + c_j^{rec} c_i^{lig} \right), \text{ and } C = \pi R_i R_j / (R_i + R_j). \text{ On equating the repulsive and attractive interaction terms, we obtain <math>h_0 \approx K(f^{ad})^2$, implying $\frac{\partial p_1}{\partial h} = \frac{J}{2C} \frac{1}{\sqrt{K}f^{ad}}$, where, $K = (B/J)^2$. Thus, the total pressure (p_t) exerted on a cell is $p_t \sim \overline{n}_{NN} \langle p_1 \rangle = \overline{n}_{NN} (h - h_0) \frac{\partial p_1}{\partial h}$, can be rewritten as,

$$p_t = (G + \lambda f^{ad}) (\mathcal{E} + \alpha f^{ad}) \left(\frac{J}{2C} \frac{1}{\sqrt{K} f^{ad}}\right),$$
 (5)

because the mean number of near-neighbors \overline{n}_{NN} increases with f^{ad} , which may be approximately written as $G + \lambda f^{ad}$ (see Fig. S2, A and B; G and λ are constants obtained from fitting simulation data). Similarly, the deviation of the cell-cell overlap from optimal packing $(h-h_0)$ increases linearly as $\mathcal{E} + \alpha f^{ad}$ (see Fig. S4; \mathcal{E}, α are constants). Notice that Eq. 5 can be written as, $\Omega p_t =$

 $(G\alpha + \lambda \mathcal{E}) + \alpha \lambda f^{ad} + \frac{G\mathcal{E}}{f^{ad}}$, where $\Omega = \left(\frac{J}{2C\sqrt{K}}\right)^{-1}$. In this form, the second term depends linearly on f^{ad} and the third is inversely proportional to f^{ad} . Since the enhancement in proliferation is maximized if the total pressure, p_t , is minimized, the minimum in the total pressure on a cell is given by the solution to $\frac{\partial p_t}{\partial f^{ad}} = 0$. Therefore, the predicted optimal cell-cell adhesion strength is $f_{opt}^{ad} = \left(\frac{G\mathcal{E}}{\alpha\lambda}\right)^{\frac{1}{2}} = 1.77 \times 10^{-4} \mu N/\mu m^2$. This is in excellent agreement with the simulation results for the peak in the tumor growth (N(t=7.5 days) in Fig. 2 D) at $f^{ad} \approx 1.75 \times 10^{-4} \mu N/\mu m^2$. More importantly, the arguments leading to Eq. 5 show that opposing contributions to the average pressure with increasing \overline{n}_{NN} and decreasing intercellular pressure at high f^{ad} drives the nonmonotonic proliferation.

Pressure-dependent mechanical feedback controls spatiotemporal proliferation patterns: Insights from simulations

We now consider how intercellular pressure varies with time and distance from the tumor center to periphery. Pressure experienced by a cell is highly dynamic, with peaks and subsequent drops in $p_i(t)$ (Fig. 3, A-C). In Fig. 3 A, black arrows highlight a switch in pressure from $p_i(t) > p_c$ (dormant phase) followed by $p_i(t) < p_c$ (growth phase). Such dynamic fluctuations in the individual cell pressure is independent of f^{ad} —as seen in Fig. 3, A-Cfor $f^{ad} = 0$, $f^{ad} = 1.5 \times 10^{-4}$, and $f^{ad} = 3 \times 10^{-4}$, Notice respectively. that, at early $0 < t \le 3.7 \tau_{min} (\sim 200,000 \text{ sec})$, pressure experienced by individual cells is lower on average compared with later times $t \gtrsim 7.4 \tau_{min} (\sim 400,000 \text{ sec})$. As the tumor cells continue to proliferate and become jammed, the pressure experienced by individual cells increases. At later times, the minimum individual pressure experienced by a cell tends to hover near the critical pressure, as indicated by the dashed line in Fig. 3, A-C.

Next, we quantified the experimentally measurable (45,46) spatial patterns in pressure experienced by cells within the MCS. The pressure on cells at the MCS center exceeds p_c (see Fig. 3 D), leading to suppressed cell growth and division. In contrast, as visualized in Fig. 3 D and quantified in Fig. 3 E, the average pressure experienced by cells close to the tumor periphery tends to be below p_c . The f^{ad} -dependent average pressure at r (distance from tumor center) is quantified using,

are most likely not dormant, in agreement with (E). (G) Proliferation rate, Γ , is enhanced at the tumor periphery, as seen in the higher values at distances r from the center of the MCS. The value of $t=12\tau_{min}$ for (E-G). (H) Average pressure experienced by cells, $\langle p \rangle$, as a function of the total number, N, of cells; $\langle p \rangle$ versus N at $f^{ad}=0$ (red; triangle), $f^{ad}=1.5\times 10^{-4}$ (blue; asterisk), and $f^{ad}=3\times 10^{-4}$ (black; squares). The corresponding double exponential fits are $[1.1\times 10^{-4}e^{5.8\times 10^{-5}\times N}-1\times 10^{-4}e^{-4.4\times 10^{-3}\times N}]$ (red line, $f^{ad}=0$), $[1.0\times 10^{-4}e^{1.7\times 10^{-5}\times N}-9.9\times 10^{-5}e^{-9.2\times 10^{-4}\times N}]$ (blue line, $f^{ad}=1.5\times 10^{-4}$), and $[1.8\times 10^{-4}e^{7.6\times 10^{-6}\times N}-1.9\times 10^{-4}e^{-9.1\times 10^{-4}\times N}]$ (black line, $f^{ad}=3\times 10^{-4}$). Inset shows N_c , the total number of cells at which the average pressure evolves to the critical pressure ($\langle p \rangle \rightarrow p_c$). To see this figure in color, go online.

$$\langle p(r) \rangle = \frac{\sum_{i} p_{i} \delta \left[r - \left(\left| \vec{R}_{CM} - \vec{r}_{i} \right| \right) \right]}{\sum_{i} \delta \left[r - \left(\left| \vec{R}_{CM} - \vec{r}_{i} \right| \right) \right]},$$
 (6)

showing that the lowest average pressure at the tumor periphery is at the intermediate value of $f^{ad} = 1.5 \times 10^{-4}$ (see Fig. 3 E). Due to the high pressure experienced by cells near the tumor center, we expect a well-defined spatial trend in the fraction of proliferating cells, F_c = $N(p_i < p_c)/N$, where $N(p_i < p_c)$ is the number of cells experiencing pressure $p_i < p_c$. Indeed, the proliferating cell fraction is low ($F_c < 0.2$) at the MCS center compared with the periphery where it approaches unity $(F_c \rightarrow 1)$, indicating that cells are in the growth/division phase (see

There is a rapid increase in F_c near the tumor periphery for $f^{ad} = 1.5 \times 10^{-4}$ (see the blue asterisks in Fig. 3 F). To better understand the spatial dependence on proliferation, we calculated the average cell proliferation rate, $\Gamma(r) = \frac{N(r,t) - N(r,t - \delta t)}{\delta t}$, where N(r,t) is the number of cells at time $t \approx 12\tau_{min}$ and $\delta t \approx 0.1\tau_{min}$ is the time interval, as a function of distance r from the tumor center. The average is over the polar and azimuthal angles, for all the cells located between distances r and $r + \delta r$ from the tumor center. Closer to the tumor center, $\Gamma(r) \sim 0$, indicating no proliferative activity. For larger values of r, approaching the MCS periphery, the proliferation rate increases rapidly. The cell proliferation rate is similar for different f^{ad} at small r (tumor core), while a much higher proliferation rate is observed for the intermediate value of f^{ad} at large r (see Fig. 3 G). The simulated spatial proliferation profile is in agreement with experimental results (45), where increased mechanical stress is correlated with lack of proliferation within the MCS, albeit when stress is exerted externally. We note that, even in the absence of an external applied stress, intercellular interactions can give rise to heterogeneity in the spatial distribution of intercellular mechanical stresses and impact spatial proliferation patterns.

Our results show that the nonmonotonic cell proliferation behavior emerges because the fraction of cells with pressure less than p_c is localized at the MCS periphery. The average pressure, $\langle p \rangle$, experienced by cells as a function of N, at the three values of f^{ad} , is shown in Fig 3 H. N_c , defined as the number of cells at which $\langle p \rangle = p_c$, exhibits a nonmonotonic behavior (inset in Fig 3 H), and supports the maximum number of cells at an intermediate f^{ad} . We surmise that, at intermediate f^{ad} , cells spatially rearrange and pack effectively to minimize the average cell pressure. For all three f^{ad} values, an initial regime where pressure rises rapidly is followed by a more gradual increase in pressure, coinciding with the exponential to power law crossover in the growth in the number of cells (see Fig. S1 A). The average pressures $(\langle p \rangle)$ as a function of N is well fit by double exponential functions (Fig 3 H). Hence, by experimentally measuring the cell proliferation rate, we can delineate the pressure sensing mechanism of cells.

Fraction of cells with pressure less than p_c controls nonmonotonic proliferation

The pressure experienced by a cell as a function of contact with other adhering cells plays an essential role in determining the observed nonmonotonic proliferation. For $f^{ad} > 0$, there is a minimum in the pressure at a nonzero cell-cell overlap distance, h_{ij} (Fig. S1 B). For instance, at $f^{ad} = 1.5 \times 10^{-4} \mu \text{N}/\mu \text{m}^2$ and $3 \times 10^{-4} \mu \text{N}/\mu \text{m}^2$, the mean pressure exerted on the cells is zero at $h_{ij} \sim 0.4 \mu \text{m}$ and $1.3 \mu \text{m}$, respectively (see Fig. S1 B). The minimum pressure is a consequence of the balance between adhesive and elastic forces. At the minimum pressure $(p_i \rightarrow 0)$, the proliferation capacity (PrC) of the cells is maximized because the cells are almost always in the growth phase. However, the impact of variations in individual cell pressure on growth of the cell collective is unclear. To determine the effect of f^{ad} on proliferation, we first quantify the spatial- and time-dependent evolution of pressure.

The fraction of cells, F_c , in the proliferating regime, corresponding to the shaded portion in Fig. 4 A exhibits a nonmonotonic behavior (inset in Fig. 4 A) with a peak at $f_c^{ad} \sim 1.75 \times 10^{-4} \mu N / \mu m^2$. The F_c value in the growth phase $(p_i < p_c)$ peaks at $\approx 38\%$, between $1 \times 10^{-4} \, \mu\text{N}/\mu\text{m}^2 < f^{ad} < 2 \times 10^{-4} \, \mu\text{N}/\mu\text{m}^2$. At lower and higher values of f^{ad} , F_c is at or below 25% on day 7.5. The inset in Fig. 4 A makes it clear that F_c , which determines the proliferative capacity of the MCS, depends nonmonotonically on f^{ad} .

The results in Fig. 2 D and the inset in Fig. 4 A suggest a phase diagram, shown in Fig. 4 B, in terms of the average cell pressure $(\langle p \rangle = \frac{\sum_i p_i}{N}$, color map) and f^{ad} . The dotted line is the boundary, $\langle p \rangle = p_c$, between the regimes where cells on average grow and divide $(p_i < p_c)$, and where they are dormant $(p_i > p_c)$. At a fixed t, the regime between $1 \times 10^{-4} \le f^{ad} \le 2 \times 10^{-4}$ shows a marked dip in the average pressure experienced by the cells. The $\langle p \rangle < p_c$ regime becomes pronounced between $2\tau_{min} \le t \le 7\tau_{min}$. In Fig. 4 C, the average pressure, $\langle p \rangle$, at $t = 6\tau_{min}$ and $12\tau_{min}$ as a function of f^{ad} , has a minimum between $f^{ad} \approx 1.5 - 2 \times 10^{-4} \mu \text{N}/\mu \text{m}^2$. Clearly, there is a close relationship between proliferation and the local pressure on a cell. As the number of cells with pressure below p_c increases, the proliferation at cell collective level is enhanced. The origin of the minimum in the average pressure at $f^{ad} = f_c^{ad}$ (Fig. 4, B and C) is less clear. The theoretical explanation for this key finding was provided above based on Eq. 5.

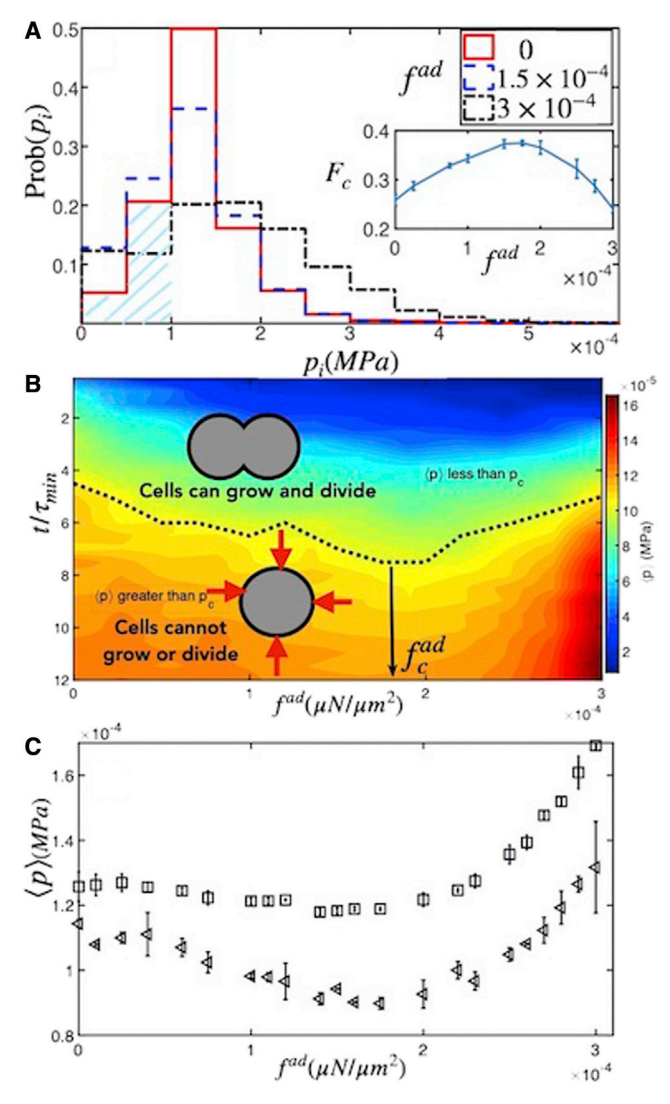


FIGURE 4 (A) The probability distribution of pressure exerted on the cell on day 7.5 for three different values of f^{ad} . The shaded regions represent cells with pressure below $p_c = 1 \times 10^{-4} \text{MPa}$. Fraction of cells (F_C) , with $p < p_c$, that grows and proliferate is shown in the inset. (B) Phase plot of the average pressure on the cells as a function of time and f^{ad} . The pressure scale is on the right. The dashed line is the boundary between the regime when cells on an average grow and divide versus the regime where mechanical pressure restricts cell growth. (C) The average pressure $\langle p \rangle$ experienced by cells at $t = 6\tau_{min}$ (left triangles, \sim day 3.75 of growth) and $t = 12\tau_{min}$ (squares, \sim day 7.5 of growth) for different values of f^{ad} . To see this figure in color, go online.

DISCUSSION

Intercellular pressure determines the biomechanical feedback

Our simulations show that nonmonotonic proliferation is determined by the fraction of proliferating cells, F_C , with pressure less than p_c . This picture is reminiscent of the mechanical feedback as a control mechanism for tissue growth proposed by Shraiman and co-workers (11,17) but with a key difference. In earlier work, cellular rearrangements do not occur readily, and the tissue is treated as an elastic sheet that resists shear (11), with mechanical stresses serving as a feedback mechanism to restrict proliferation. In our case, large-scale cell rearrangements are possible (34) as a cell or group of cells could go in and out of dormancy. Despite the differences, the idea that local pressure serves as a regulatory mechanism of growth could be a general feature of mechanical feedback (11), as we show below based on analysis of experimental data.

Agreement between simulation predictions and experimental data indicate that the pressureadhesion feedback loop determines cell proliferation in complex in vivo cell collectives

We now analyze experimental data in light of predictions from our simulations. Based on the observation of enhanced cell migration at low E-cadherin levels, tumor invasion and metastasis is considered to be a consequence of loss of E-cadherin expression (47). However, most breast cancer primary and metastatic tumors express E-cadherin (48). Our simulations suggest that tumor spheroids made up of cells with higher E-cadherin expression (E-cad(control)) grow ≈ 1.9 times faster compared with tumor spheroids made up of low E-cadherin (E-cad(-)) expressing cells (see Fig. 5 A), in reasonable agreement with experiments (44). Comparison of the tumor diameter growth between E-cad(-) cells and E-cad(control) (red and blue lines, respectively, Fig. 5 A) shows enhanced growth rates for E-cad(control) cells at t > 4 days. The linear fit for the simulated tumor diameter growth rate is obtained by analyzing data at t > 4 days (dashed lines, Fig. 5 A). The growth rate ratio is then calculated by taking the ratio of the slope of the two diameter growth lines.

Padmanaban et al. (44) compared the tumor growth behavior between E-cadherin-expressing cells (control) and E-cadherin-negative cells (characterized by reduced E-cadherin expression compared with control) using 3D tumor organoids. They conclude that tumors arising from low E-cadherin-expressing cells (E-cad(-)) were smaller than tumors from control E-cadherin (E-cad(control)) expressing cells at corresponding time points over multiple weeks of tumor growth (see Fig. 5 B). By extracting the tumor growth rate for E-cad(-) and E-cad(control) organoids from the experimental data (44), the longest tumor dimension for E-cad(control) tumor organoids expanded ≈ 1.3 times faster compared with E-cad(-) tumor organoids (see Fig. 5 B). Both the linear functional form of the tumor growth rates and the higher growth rates in E-cad(control) tumor spheroids as compared with E-cad(-) tumor spheroids are in reasonable agreement with the simulations. It is worth emphasizing that the simulation results were obtained without any fits to the experiments (44).

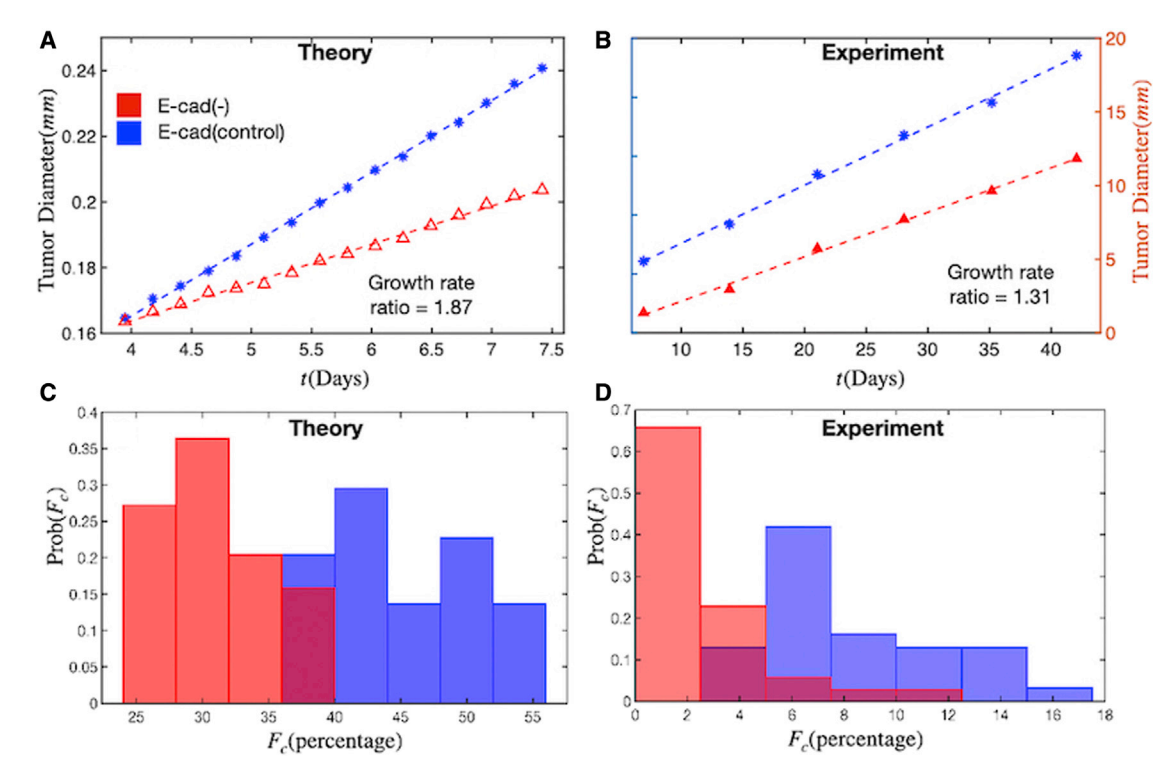


FIGURE 5 Pressure-adhesion feedback loop determines cell proliferation in complex in vivo cell collectives: (A) kinetics of growth in the diameter of the MCS composed of cells with low E-cadherin expression (red; $f^{ad}=0$; E-cad(-)) and intermediate E-cadherin expression (blue; $f^{ad}=1.75\times10^{-4}$; E-cad(control)) from simulations show enhanced tumor growth rate due to higher E-cadherin expression. The tumor diameter growth is linear at t > 4days for both E-cadherin expression levels considered. However, the growth rate of the tumor colony at intermediate E-cadherin expression is larger, in agreement with experimental results. (B) Growth rates of the longest tumor dimension in low E-cadherin-expressing organoids compared with control organoids with normal E-cadherin expression from experimental data (data were extracted from (44)). (C) Calculated probability distribution of the mitotic fraction, F_C, in cell colonies expressed as percent for low E-cadherin tumor MCS (red) and normal E-cadherin-expressing tumor MCS (blue) shows enhanced proliferation capacity when E-cadherin expression is increased. (D) In agreement with our prediction, the probability distribution of the mitotic fraction, F_C , for low E-cadherin tumor organoids (red) and normal E-cadherin-expressing tumor organoids (blue) shows enhanced proliferation capacity at higher E-cadherin expression. Data were extracted from experiments (see the supporting material data in Table 3e in the experimental report (44)). Although there is paucity of experimental data, it is encouraging that the currently available measurements are in line with our predictions. To see this figure in color, go online.

To ensure that the difference in tumor growth rate is due to differences in cell proliferation, we analyzed the ratio of the number of actively dividing cells to the total number of cells (referred to as mitotic fraction) with experimental data obtained from staining tumor cell colonies for PH3 (phospho-histone 3; a mitotic marker). As predicted, E-cadherin-expressing tumor cell colonies have a larger mitotic fraction (blue histogram, Fig. 5 C) compared with low E-cadherin-expressing tumor cells (red histogram, Fig. 5 C). We compare the mitotic fraction, F_C , in E-cad(-) and E-cad(control) in the Fig. 5, C and D between theory and experiment. In agreement with our simulation predictions, enhanced mitotic fraction is seen in tumor organoids with normal E-cad expression (44) (see Fig. 5 D).

CONCLUSIONS

We have established that increasing cell-cell adhesion strength contributes to mechanical pressure based inhibition of cell growth and proliferation. Surprisingly, growth of the MCS exhibits a nonmonotonic behavior as a function of increasing cell adhesion strength. Cell-cell adhesion strength and critical pressure based inhibition of cell growth qualitatively captures cell proliferation patterns observed in the context of cancer progression. The observed role of E-cadherin in tumor growth could be related to a feedback mechanism due to changes in local pressure as the cellcell interaction strength is varied. The pressure feedback on the growth of cells accounts for cell proliferation in the simulations. In agreement with previous work connecting cell-cell adhesion to unjamming (49), our results suggest that the role of adhesion in tissue behavior is indeed rich and result in complex behaviors.

In actuality, it may well be that mechanical forces do not directly translate into proliferative effects. Rather, cell-cell contact (experimentally measurable through the contact length l_c , for example) could biochemically regulate cell signaling (e.g., Rac1/RhoA), which in turn controls proliferation, as observed in biphasic proliferation of cell collectives in both two and three dimensions (50, 51). Nevertheless, contact inhibition of proliferation, based on mechanical pressure experienced by single cells can be captured using a pressure-based feedback on proliferation in computer simulations. Such mechanical control of proliferation could be a generic mechanism governing how cell-cell adhesion strength, acting on the scale of at best few microns, affects tumor growth that occurs on the scale of millimeters.

SUPPORTING MATERIAL

Supporting material can be found online at https://doi.org/10.1016/j.bpj. 2022.04.032.

AUTHOR CONTRIBUTIONS

A.N.M.-K. and D.T. designed the research. A.N.M.-K., S.S., and X.L. performed the research. A.N.M.-K. analyzed the data with inputs from D.T., S.S., and X.L. A.N.M.-K., D.T., S.S., and X.L. wrote the paper.

DECLARATION OF INTERESTS

The authors declare no competing interests.

ACKNOWLEDGMENTS

We acknowledge Anne D. Bowen at the Visualization Laboratory (Vislab), Texas Advanced Computing Center, for help with video visualizations. We are grateful to Dr. Andrew Ewald, Dr. Tony Tsai, Dr. Robert Huebner, and Dr. Paul Langridge for discussions. This work is supported by the National Science Foundation (PHY 17-08128) and the Collie-Welch Chair through the Welch Foundation (F-0019). A.N.M.-K. acknowledges funding support from the College of Science and Mathematics at Augusta University. The authors declare that they have no conflict of interest.

REFERENCES

- Thompson, D. W. 1942. On Growth and Form2. Cambridge Univ. Press. https://doi.org/10.1017/CBO9781107325852.
- Shaw, T. J., and P. Martin. 2009. Wound repair at a glance. J. Cell Sci. 122:3209–3213. https://doi.org/10.1242/jcs.031187.
- Chen, Y., L. Ju, ..., C. Zhu. 2017. Receptor-mediated cell mechanosensing. *Mol. Biol. Cell.* 28:3134–3155. https://doi.org/10.1091/mbc.e17-04-0228.
- Chen, Y., Z. Li, and L. A. Ju. 2019. Tensile and compressive force regulation on cell mechanosensing. *Biophysical Rev.* 11:311–318. https://doi.org/10.1007/s12551-019-00536-z.
- Kamkin, A. G., and I. S. Kiseleva. 2005. Mechanosensitivity in Cells and Tissues. Springer, pp. 171–172.
- Delarue, M., J. Hartung, ..., O. Hallatschek. 2016. Self-driven jamming in growing microbial populations. *Nat. Phys.* 12:762–766. https://doi. org/10.1038/nphys3741.
- Gniewek, P., C. F. Schreck, and O. Hallatschek. 2019. Biomechanical feedback strengthens jammed cellular packings. *Phys. Rev. Lett.* 122:208102. https://doi.org/10.1103/physrevlett.122.208102.
- 8. Abercrombie, M. 1970. Contact inhibition in tissue culture. *In vitro*. 6:128–142. https://doi.org/10.1007/bf02616114.
- Folkman, J., and A. Moscona. 1978. Role of cell shape in growth control. *Nature*. 273:345–349. https://doi.org/10.1038/273345a0.
- Chen, C. S., M. Mrksich, ..., D. E. Ingber. 1997. Geometric control of cell life and death. *Science*. 276:1425–1428. https://doi.org/10.1126/ science.276.5317.1425.

- Shraiman, B. I. 2005. Mechanical feedback as a possible regulator of tissue growth. *Proc. Natl. Acad. Sci. U S A.* 102:3318–3323. https://doi.org/10.1073/pnas.0404782102.
- Streichan, S. J., C. R. Hoerner, ..., L. Hufnagel. 2014. Spatial constraints control cell proliferation in tissues. *Proc. Natl. Acad. Sci. U S A*. 111:5586–5591. https://doi.org/10.1073/pnas.1323016111.
- Jacobeen, S., J. T. Pentz, ..., P. J. Yunker. 2018. Cellular packing, mechanical stress and the evolution of multicellularity. *Nat. Phys.* 14:286–290. https://doi.org/10.1038/s41567-017-0002-y.
- Puliafito, A., L. Hufnagel, ..., B. I. Shraiman. 2012. Collective and single cell behavior in epithelial contact inhibition. *Proc. Natl. Acad. Sci. U S A*. 109:739–744. https://doi.org/10.1073/pnas.1007809109.
- McClatchey, A. I., and A. S. Yap. 2012. Contact inhibition (of proliferation) redux. *Curr. Opin. Cell Biol.* 24:685–694. https://doi.org/10.1016/j.ceb.2012.06.009.
- Kourtidis, A., R. Lu, ..., P. Z. Anastasiadis. 2017. A central role for cadherin signaling in cancer. *Exp. Cell Res.* 358:78–85. https://doi. org/10.1016/j.yexcr.2017.04.006.
- Irvine, K. D., and B. I. Shraiman. 2017. Mechanical control of growth: ideas, facts and challenges. *Development*. 144:4238–4248. https://doi. org/10.1242/dev.151902.
- 18. LeGoff, L., and T. Lecuit. 2016. Mechanical forces and growth in animal tissues. *Cold Spring Harbor Perspect. Biol.* 8:a019232.
- Friedl, P., and R. Mayor. 2017. Tuning collective cell migration by cell-cell junction regulation. *Cold Spring Harbor Perspect. Biol.* 9:a029199.
- Takeichi, M. 1988. The cadherins: cell-cell adhesion molecules controlling animal morphogenesis. *Development*. 102:639–655.
- Saito, M., D. K. Tucker, ..., A. P. Kowalczyk. 2012. Classical and desmosomal cadherins at a glance. J. Cell Sci. 125:2547–2552. https://doi.org/10.1242/jcs.066654.
- Halbleib, J. M., and W. J. Nelson. 2006. Cadherins in development: cell adhesion, sorting, and tissue morphogenesis. *Genes Dev.* 20:3199– 3214. https://doi.org/10.1101/gad.1486806.
- Van Roy, F., and G. Berx. 2008. The cell-cell adhesion molecule E-cadherin. Cell Mol. Life Sci. 65:3756–3788.
- Tabdanov, E., N. Borghi, ..., J.-P. Thiery. 2009. Role of E-cadherin in membrane-cortex interaction probed by nanotube extrusion. *Biophysical J.* 96:2457–2465. https://doi.org/10.1016/j.bpj.2008.11. 059.
- Borghi, N., M. Sorokina, ..., A. R. Dunn. 2012. E-cadherin is under constitutive actomyosin-generated tension that is increased at cellcell contacts upon externally applied stretch. *Proc. Natl. Acad. Sci.* U S A. 109:12568–12573. https://doi.org/10.1073/pnas.1204390109.
- Shams, H., M. Soheilypour, ..., M. R. Mofrad. 2017. Looking "under the Hood" of cellular Mechanotransduction with computational tools: a systems biomechanics approach across multiple scales. ACS Biomater. Sci. Eng. 3:2712–2726.
- Yap, A. S., G. A. Gomez, and R. G. Parton. 2015. Adherens junctions revisualized: organizing cadherins as nanoassemblies. *Dev. Cell*. 35:12–20.
- Amack, J. D., and M. L. Manning. 2012. Knowing the boundaries: extending the differential adhesion hypothesis in embryonic cell sorting. *Science*. 338:212–215. https://doi.org/10.1126/science.1223953.
- David, R., O. Luu, ..., R. Winklbauer. 2014. Tissue cohesion and the mechanics of cell rearrangement. *Development*. 141:3672–3682. https://doi.org/10.1242/dev.104315.
- Schaller, G., and M. Meyer-Hermann. 2005. Multicellular tumor spheroid in an off-lattice Voronoi-Delaunay cell model. *Phys. Rev. E*. 71:051910. https://doi.org/10.1103/PhysRevE.71.051910.
- Drasdo, D., and S. Höhme. 2005. A single-cell-based model of tumor growth in vitro: monolayers and spheroids. *Phys. Biol.* 2:133–147. https://doi.org/10.1088/1478-3975/2/3/001.
- Galle, J., M. Loeffler, and D. Drasdo. 2005. Modeling the effect of deregulated proliferation and apoptosis on the growth dynamics of

- epithelial cell populations in vitro. Biophysical J. 88:62-75. https://doi. org/10.1529/biophysj.104.041459.
- 33. Li, J., S. K. Schnyder, ..., R. Yamamoto. 2021. Role of the cell cycle in collective cell dynamics. Phys. Rev. X. 11:031025.
- 34. Malmi-Kakkada, A. N., X. Li, ..., D. Thirumalai. 2018. Cell growth rate dictates the onset of glass to fluidlike transition and long time superdiffusion in an evolving cell colony. Phys. Rev. X. 8:021025.
- 35. Sinha, S., A. N. Malmi-Kakkada, ..., D. Thirumalai. 2020. Spatially heterogeneous dynamics of cells in a growing tumor spheroid: comparison between theory and experiments. Soft Matter. 16:5294–5304. https://doi.org/10.1039/c9sm02277e.
- 36. Sinha, S., and D. Thirumalai. 2020. Self-generated persistent random forces drive phase separation in growing tumors. J. Chem. Phys. 153:201101. https://doi.org/10.1063/5.0026590.
- 37. Sinha, S., and A. N. Malmi-Kakkada. 2021. Inter-particle adhesion regulates the surface roughness of growing dense three-dimensional active particle aggregates. J. Phys. Chem. B. 125:10445-10451.
- 38. Dammer, U., O. Popescu, ..., G. Misevic. 1995. Binding strength between cell-adhesion proteoglycans measured by Atomic-force microscopy. Science. 267:1173-1175.
- 39. Baronsky, T., A. Dzementsei, ..., A. Janshoff. 2016. Reduction in E-cadherin expression fosters migration of Xenopus laevis primordial germ cells. Integr. Biol. 8:349-358. https://doi.org/10. 1039/c5ib00291e.
- 40. Maître, J.-L., H. Berthoumieux, ..., C.-P. Heisenberg. 2012. Adhesion functions in cell sorting by mechanically coupling the cortices of adhering cells. science. 338:253-256. https://doi.org/10.1126/science.
- 41. Petridou, N. I., B. Corominas-Murtra, ..., E. Hannezo. 2021. Rigidity percolation uncovers a structural basis for embryonic tissue phase transitions. Cell. 184:1914-1928.

- 42. Di Meglio, I., A. Trushko, ..., A. Roux. 2021. Pressure and curvature control of contact inhibition in epithelia growing under spherical confinement. Preprint at bioRxiv.
- 43. Lewis-Tuffin, L. J., F. Rodriguez, ..., P. Z. Anastasiadis. 2010. Misregulated E-cadherin expression associated with an aggressive brain tumor phenotype. PLoS One. 5:e13665. https://doi.org/10.1371/journal. pone 0013665.
- 44. Padmanaban, V., I. Krol, ..., A. J. Ewald. 2019. E-cadherin is required for metastasis in multiple models of breast cancer. Nature. 573:439-444. https://doi.org/10.1038/s41586-019-1526-3.
- 45. Dolega, M. E., M. Delarue, ..., G. Cappello. 2017. Cell-like pressure sensors reveal increase of mechanical stress towards the core of multicellular spheroids under compression. Nat. Commun. 8:14056. https:// doi.org/10.1038/ncomms14056.
- 46. Mongera, A., P. Rowghanian, ..., O. Campàs. 2018. A fluid-to-solid jamming transition underlies vertebrate body axis elongation. Nature. 561:401–405. https://doi.org/10.1038/s41586-018-0479-2.
- 47. Frixen, U. H., J. Behrens, ..., W. Birchmeier. 1991. E-cadherin-mediated cell-cell adhesion prevents invasiveness of human carcinoma cells. J. Cell Biol. 113:173-185. https://doi.org/10.1083/jcb.113.1.173.
- 48. Li, C. I., B. O. Anderson, ..., R. E. Moe. 2003. Trends in incidence rates of invasive lobular and ductal breast carcinoma. Jama. 289:1421–1424. https://doi.org/10.1001/jama.289.11.1421.
- 49. Bi, D., J. Lopez, J. M. Schwarz, and M. L. Manning. 2015. A densityindependent rigidity transition in biological tissues. Nat. Phys. 11:1074-1079
- 50. Liu, W. F., C. M. Nelson, ..., C. S. Chen. 2006. E-cadherin engagement stimulates proliferation via Rac1. J. Cell Biol. 173:431-441. https:// doi.org/10.1083/jcb.200510087.
- 51. Gray, D. S., W. F. Liu, ..., C. S. Chen. 2008. Engineering amount of cell-cell contact demonstrates biphasic proliferative regulation through RhoA and the actin cytoskeleton. Exp. Cell Res. 314:2846–2854. https://doi.org/10.1016/j.yexcr.2008.06.023.